

Article

# Autonomous Navigation UAVs for Enhancing Information Freshness for Reconnaissance

Chen Xie <sup>1</sup>, Binbin Wu <sup>1</sup>, Daoxing Guo <sup>1,\*</sup> and Xiao Chen <sup>2</sup>

<sup>1</sup> The College of Communications Engineering, PLA Army Engineering University, Nanjing 210007, China; 17715260518@126.com (C.X.); wbb919@126.com (B.W.)

<sup>2</sup> The School of Artificial Intelligence/School of Future Technology, Nanjing University of Information Science and Technology, Nanjing 210044, China; x.chen@nuist.edu.cn

\* Correspondence: xyzgfg@sina.com

**Abstract:** The demand for autonomous navigation UAVs in reconnaissance is steadily increasing. One crucial aspect of these missions is the freshness of reconnaissance information, which serves as a vital indicator of mission effectiveness. However, there is a lack of targeted investigation in the research on autonomous single/multi-UAV missions and joint path planning. Furthermore, the use of visual-inertial odometry (VIO) in rotary-wing UAVs can lead to significant positional drift during flight, which may result in the loss of the UAV and mission failure. This paper investigates joint planning problems in single/multi-UAV reconnaissance missions under both GPS-available and GPS-unavailable scenarios and proposes an integrated data collection and beacon-assisted localization approach. Finally, the numerical results demonstrate the effectiveness of the proposed scheme in enhancing the freshness of reconnaissance information.

**Keywords:** unmanned aerial vehicle; autonomous UAVs; reconnaissance; data collection; mission planning; path planning; heuristic optimization; information freshness; localization drift



**Citation:** Xie, C.; Wu, B.; Guo, D.; Chen, X. Autonomous Navigation UAVs for Enhancing Information Freshness for Reconnaissance. *Electronics* **2024**, *13*, 1354. <https://doi.org/10.3390/electronics13071354>

Academic Editor: Felipe Jiménez

Received: 29 February 2024

Revised: 31 March 2024

Accepted: 2 April 2024

Published: 3 April 2024



**Copyright:** © 2024 by the authors. Licensee MDPI, Basel, Switzerland. This article is an open access article distributed under the terms and conditions of the Creative Commons Attribution (CC BY) license (<https://creativecommons.org/licenses/by/4.0/>).

## 1. Introduction

Smart unmanned systems are playing an increasingly significant role in various fields, such as space exploration, intelligent industry, and modern warfare [1]. Among them, small/micro unmanned aerial vehicles (UAVs) exhibit the highest flexibility in three-dimensional movement in low-altitude environments. Compared to traditional reconnaissance methods, utilizing UAVs to perform direct aerial reconnaissance or to assist ground reconnaissance nodes in data collection has advantages [2]. The former allows onboard terminals to capture information with vertical dimensions in real space [3]. However, this requires lightweight equipment due to payload limitations. While ground reconnaissance nodes can reliably obtain real-time information within their perception area, establishing real-time communication links with the backend data center is still challenging due to limitations in wireless communication power, complex channel conditions, and concerns about concealment [4–6]. Utilizing UAVs to collect data from reconnaissance nodes and bring them to the data center for decision-making can effectively solve the communication problem [7]. Nevertheless, collision risks and electromagnetic interference pose a threat in practice, while the missions are highly complex. Therefore, autonomous UAVs with well-designed planners are essential for this scenario [8], while data collection by UAVs from ground nodes in close range increases the signal-to-noise ratio under limited communication power.

In actual reconnaissance missions, signal interference and radio hijacking can result in UAVs being unable to receive the correct remote control signals and can hinder accurate satellite positioning signal reception, leading to the possibility of UAVs crashing or being intercepted. Additionally, other types of interference, such as acoustic interference, can

prevent UAVs from utilizing acoustic sensors for environmental awareness and sound-based positioning. To address these issues, drawing inspiration from the general framework and autonomous capabilities of current small/micro rotary-wing UAVs, this paper presents a solution based on autonomous UAVs: UAVs that can successfully complete assigned missions and achieve objectives without human intervention, autonomously determining their waypoints and guiding movement based on available environmental and mission information. The functional modules required to achieve autonomous navigation include mission and path planning, perception and localization, and flight control. Among them, the planner serves as the core of autonomous UAVs.

For autonomous path planning in environments with dense obstacles, Zhou et al. proposed a framework that includes visual cameras, an inertial measurement unit (IMU), simultaneous localization and mapping (SLMM), a motion planner, and a cooperative locator [9]. The objective of the planning is to minimize the flight time, ensuring effective obstacle avoidance for unexpected obstacles and seamless local trajectory adjustments. Similarly, in [10,11], the problem of minimum-flight-time motion planning for point-to-point navigation is addressed. However, in scenarios with a large number of ground reconnaissance nodes, point-to-point motion planning may struggle to meet the overall requirements for the freshness of reconnaissance information. Therefore, the planner must conduct a coordinated optimization of both the waypoints' access order and the UAV's flight trajectory. Furthermore, in GPS-denied scenarios, although multi-UAV formation flying with an advanced visual + ultra-wideband (UWB) cooperative inter-vehicle positioning design can reduce the cumulative positioning error of individual UAVs using autonomous visual-inertial odometry (VIO) positioning, there is still nearly 1 m of position drift every 100 m of flight [12]. Additionally, multi-UAV cooperative localization is often impractical due to reduced mission efficiency [13–15]. Therefore, under normal circumstances, the UAV position drift can reach nearly 3 m or even more every 100 m [12]. The position drift can lead to UAV position loss, causing mission failure and a UAV crash. This paper proposes an approach to address the position drift using the planner of the UAV, aiming to offer an innovative solution.

B. Miloradovic et al. [16] designed a planner based on an improved genetic algorithm, which performs the joint optimization of the total flight time and total mission duration under heterogeneous mission constraints. By solving the established extended colored traveling salesman problem (ECTSP) model, the freshness of reconnaissance information is improved. H. Hu et al. [17] provided a clear definition of the age of information (AoI) for nodes in a scenario of UAV-assisted data collection, effectively characterizing the freshness of reconnaissance information. In this kind of scenario [18], the joint planning of the UAV mission assignment, node access sequence optimization, and trajectory generation plays a dominant role in the overall freshness of reconnaissance information. Therefore, research such as [19] has studied the joint planning problem within a unified framework. Although the aforementioned studies have considered the heterogeneity of nodes, in practical applications, different types of reconnaissance data have heterogeneous levels of information urgency, which need to be considered in the joint planning problem.

To address the aforementioned challenges, we developed a UAV flight planner that effectively collects data from ground reconnaissance nodes, enabling the efficient reconnaissance of a specific area and optimizing the overall freshness of reconnaissance information. In a mountainous environment with no-fly zones, we deployed several ground reconnaissance nodes with known coordinates, each with a different data volume and urgency. The proposed algorithm was designed and improved based on classical heuristic algorithms, such as the genetic algorithm. Furthermore, we designed a flight planning method for both GPS-enabled and GPS-denied environments, building upon popular VIO navigation. In the proposed framework, we integrated data collection and beacon-assisted localization to mitigate the VIO position drift when GPS is unavailable due to signal interference or hijacking. Additionally, we compared our planner with other schemes for improving information freshness, further highlighting the superiority of the proposed framework.

## 2. System Model

In order to achieve the effective reconnaissance of a specific mission area, we deployed  $N$  ground reconnaissance nodes with known coordinates within the area, denoted by  $S = \{s_1, \dots, s_n, \dots, s_N\}$ . Their coordinates are, respectively, denoted by  $\omega_n = (x_n, y_n, h_n)$ , where  $n = 1, 2, \dots, N$ . Due to the difficulty of direct communication between reconnaissance nodes and the data center, single or multiple UAVs are dispatched from the data center to fly to a hovering position directly above each reconnaissance node. The UAV maintains a hovering flight and sends data collection instructions to the nodes. After the data collection is completed, the UAV moves on to the next node and eventually returns to the data center to unload the collected data, completing the information retrieval process. The coordinates of the data center  $s_{dc}$  are denoted by  $\omega_{dc} = (x_{dc}, y_{dc}, h_{dc})$ . When a single UAV is used for data collection, it is denoted by  $v$ . In the case of multiple UAVs being used for data collection, the set of UAVs is denoted by  $\mathcal{V} = \{v_1, \dots, v_m, \dots, v_M\}$ , where  $m = 1, 2, \dots, M$ , and  $M$  represents the total number of UAVs.

### 2.1. Age of Reconnaissance Information and Information Urgency

The ground reconnaissance node  $s_n$  continuously acquires information before receiving data collection instructions from the UAV. It also broadcasts positioning signals to the surrounding area to assist the UAV in location calibration, thereby eliminating the position drift caused by accumulated errors. Once  $s_n$  receives the data collection instructions, it immediately starts uploading the reconnaissance data, and this time is defined as the information effective timestamp [17], denoted by  $T_{m,n}$ . The AoI of  $s_n$  is

$$\Delta_{(n)}(t) = (t - T_{m,n})^+ \tag{1}$$

where  $(\alpha)^+ = \max\{0, \alpha\}$ .

However, considering the fact that the data collected by ground sensors in actual reconnaissance missions may be of different types, it is necessary to take into account the heterogeneity of information urgency when optimizing the average AoI (AAoI) of all nodes. This can be achieved by using a non-negative and monotonically increasing cost function to describe the rate of heterogeneous AoI growth.

When  $\alpha > 0$ , the cost function, which represents the freshness of information, also known as the AoI function, exhibits an exponential growth rate. This is because, for reconnaissance information with higher urgency, the mutual information decreases rapidly after a certain amount of time elapses, which is mainly due to the flight time of the unmanned aerial vehicle and data transmission. Conversely, for data types with slower mutual information decay, setting  $\alpha < 0$  allows the reconnaissance information to decay at a logarithmic rate. For data types with moderate urgency, general linear growth is adopted, i.e.,  $\alpha \rightarrow 0$ , as shown in Figure 1. In the time scale range of the application in this paper, the parameter settings in the figure cause different types of reconnaissance information to exhibit exponential growth, linear growth, and logarithmic growth in terms of AoI.

$$f_k(t) \triangleq \alpha_k^{-1} (e^{\alpha_k t} - 1) \tag{2}$$

which extends the typical AoI to a generalized non-linear form [20].

Assuming that  $s_{m,i}$  represents the  $i$ -th reconnaissance node accessed by  $v_m$ , the AoI is considered to be 0 before accessing that particular node. The AoI starts to increase when  $s_i$  begins to upload data, specifically after time  $T_{m,i}$ . The computational model is illustrated in Figure 2. At time  $T_{m,i+1}$ , the AoI of  $s_{m,i}$  is

$$\begin{aligned} \Delta_{(m,i)}^*(T_{m,i+1}) &= f_k(t_{(i)}^{dc} + t_{(i)}^f) \\ &= \alpha_k^{-1} \left( e^{\alpha_k (t_{(i)}^{dc} + t_{(i)}^f)} - 1 \right) \end{aligned} \tag{3}$$

where the selection of the parameter  $\alpha_k$  depends on the type of current node and its degree of information urgency.

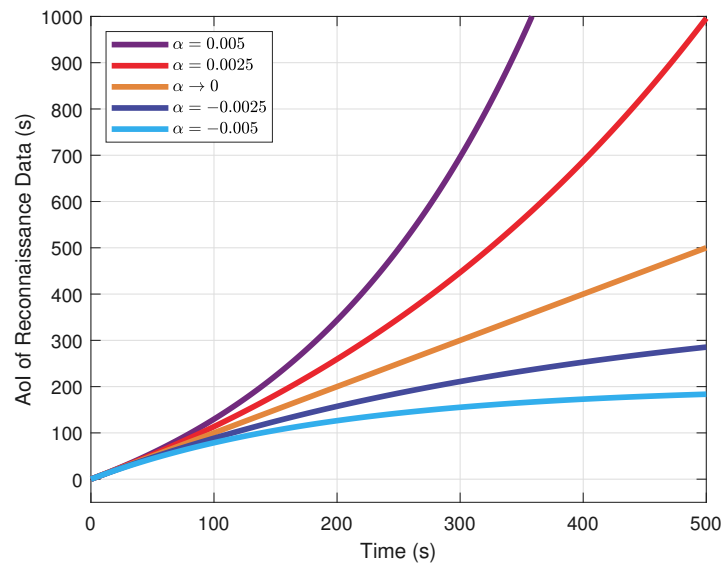


Figure 1. The AoI growth rates of different types of reconnaissance nodes.

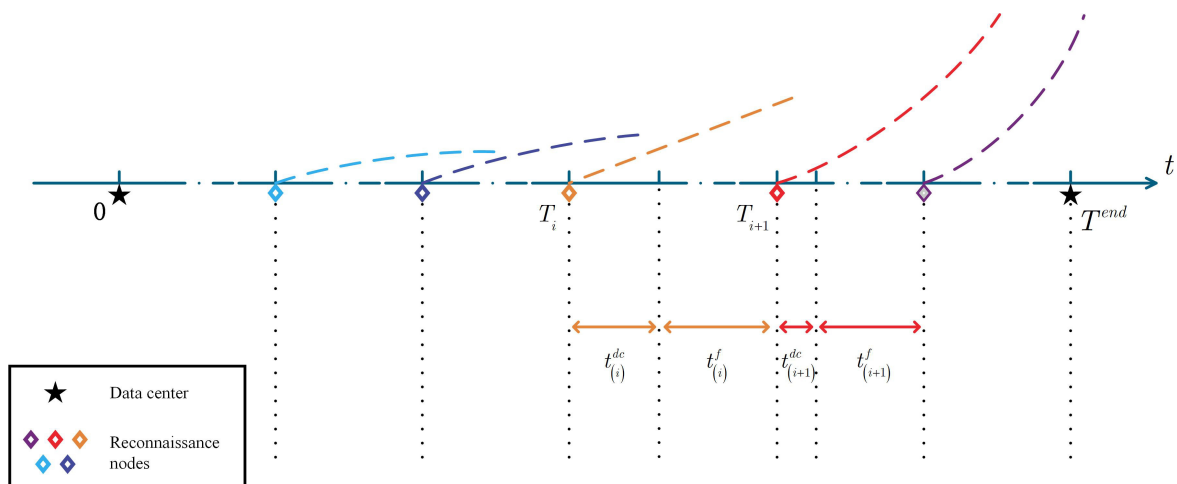


Figure 2. AoI model for reconnaissance nodes with heterogeneous urgency.

2.2. Reconnaissance Data Collection Model

The communication channel between the UAV and the ground reconnaissance node is characterized by the Rician fading channel model [21–23], where the power decay coefficient per unit distance is denoted by  $\mu_0$ , and the path fading exponent is denoted by  $2 \leq \alpha \leq 5.5$ . The data transmission rate between the UAV and the ground reconnaissance node is denoted by

$$R_t = B \log_2 \left( 1 + \frac{p_t \gamma d_c^{-\alpha}}{\sigma^2} \right) \tag{4}$$

where  $B$  represents the data transmission bandwidth,  $p_t$  represents the transmission power of the reconnaissance node,  $d_c$  is the maximum communication range between the UAV and the node, and  $\gamma$  is calculated as follows:

$$\gamma = \frac{1}{B\Gamma} \left[ \frac{\mathcal{F}}{\mathcal{F} + 1} \mu_0 + \frac{1}{\mathcal{F} + 1} \mu_0 |\tilde{h}_c|^2 \right] \tag{5}$$

where  $\Gamma$  represents the efficiency caused by modulation and coding,  $\mathcal{F}$  represents the environmental parameter that characterizes the line-of-sight (LoS) channel probability between the UAV and the reconnaissance node, and  $\tilde{h}_c$  represents a random non-line-of-sight (NLoS) channel.

In addition, the received signal power at the data collection terminal is

$$p_r = p_t \gamma d_c^{-\alpha} \quad (6)$$

while the receiver sensitivity is

$$p_0 = k_b T_0 \times N_f \times R_{\min} \times \frac{E_b}{N_0} \quad (7)$$

where  $k_b$  is the Boltzmann constant,  $T_0$  is the ambient temperature,  $N_f$  is the RF circuit noise factor,  $R_{\min}$  is the minimum communication rate, and  $E_b/N_0$  is the normalized demodulation threshold. Therefore, the minimum data collection rate constraint and minimum received power constraint are established as follows:

$$R_t \geq R_{\min} \quad (8)$$

$$p_r \geq p_0. \quad (9)$$

### 2.3. Integrated Data Collection with Beacon-Assisted Localization

VIO provides real-time and accurate localization information for autonomous UAVs. However, the coordinates provided by VIO are relative to the take-off position of the UAV, leading to challenging position drift issues. Specifically, the SLMM module utilizes multiple frame images captured by visual sensors to solve the current position of the UAV based on the inter-frame positional transformation. In large-scale reconnaissance scenarios, the localization errors introduced by visual sensors and position estimation algorithms accumulate over time, causing a position drift. Similarly, the IMU module calculates the position based on the acceleration changes sensed by the gyroscope during the UAV motion, resulting in the accumulation of errors introduced by the sensor and estimation algorithms during flight.

The VIO position drift can cause the UAV to reach a spherical trust region with a radius of  $r_0$  around the predetermined coordinates, rather than precisely reaching the intended location after a certain period of flight time.  $r_0$  is typically an empirical parameter obtained from experiments, representing the upper limit of the VIO position drift [9]. The magnitude of  $r_0$  is dependent on the total distance traveled by the UAV from its starting point. When  $r_0$  exceeds a certain range, the UAV may not be able to locate the reconnaissance nodes after reaching the designated coordinates. Additionally, excessive self-positioning errors can lead to mission failures or even result in the loss of the UAV.

Therefore, when satellite positioning signals are available, the UAV can utilize GPS positioning at a certain frequency to correct accumulated VIO errors. In this case, the mission and path planning of autonomous UAVs only need to consider conventional safety constraints and the optimization of reconnaissance mission indicators. However, in GPS-denied environments, where satellite positioning is not available, it is hard to eliminate the position drift. To address this issue, we propose an integrated solution for reconnaissance data collection and beacon-assisted positioning, as shown in Figure 3. In large-scale reconnaissance areas, the position drift of VIO typically occurs in the horizontal latitude and longitude coordinates. Therefore, when the UAV flies toward ground reconnaissance nodes with known coordinates, the UAV position can be corrected using the horizontal coordinates of the ground reconnaissance nodes as well as the relative position information between the UAV and the nodes [24,25].

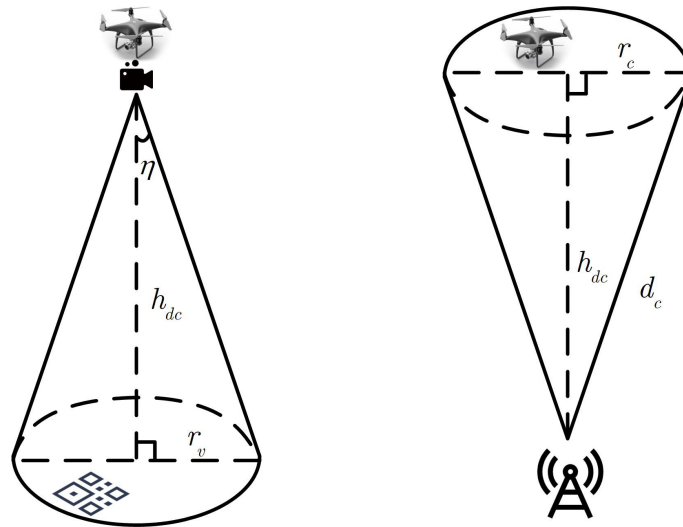


**Figure 3.** The integrated solution for reconnaissance data collection and beacon-assisted positioning, which includes visual beacon positioning correction (left) and wireless beacon positioning correction (right).

This solution combines two correction methods. The left image in Figure 3 illustrates visual beacon positioning correction. It involves placing markers resembling 2D barcodes, known as AprilTag, on the ground reconnaissance nodes. These tags provide visual guidance to the UAV, helping to correct cumulative errors. Here,  $\eta$  represents the half-field angle of the UAV’s downward-facing camera, and  $r_{c1}$  is the error tolerance radius, satisfying

$$r_{c1} = h_{dc} \tan(\eta) \tag{10}$$

where  $h_{dc}$  represents the hovering height of the UAV during data collection from the ground reconnaissance nodes, and it must satisfy the following constraint:

$$h_{dc} < d_c \tag{11}$$

When the horizontal position drift of the UAV is smaller than the error tolerance radius, the AprilTag marker falls within the field of view, and beacon-assisted positioning is successful.

The right image in Figure 3 shows the wireless beacon positioning correction. When the UAV reaches the vicinity of the node and receives the wireless signal, it can use the positioning information for position correction. The error tolerance radius for this method is represented by

$$r_{c2} = \|d_c - h_{dc}\| \tag{12}$$

Therefore, when the UAV reaches the hovering collection position of a reconnaissance node, its horizontal coordinates must fall within a circle with the horizontal coordinates of the reconnaissance node as the center and  $\max(r_{c1}, r_{c2})$  as the radius. Otherwise, it will result in a loss of positioning.

#### 2.4. Safe Flight of Autonomous Reconnaissance UAVs

In practical UAV trajectory planning, digital elevation models (DEMs) are widely used to describe terrain features. In complex mountainous environments, the flight path of the UAV must avoid collisions with the ground while adhering to constraints on the maximum flying height. Therefore, the obtained open-source DEM is discretized into a grid map using rasterization methods, and a point-to-point optimal flight trajectory is generated based on this map. This process results in a topological map of the UAV flight and the flight time cost between each pair of hover points, which is used to calculate the AoI of the reconnaissance node considering heterogeneous information urgency.

Additionally, we also consider no-fly zones, interference zones, and other regions that pose safety threats, modeling them as cylindrical zones. These zones, along with terrain data, generate three-dimensional grid occupancy information within the mission area, which is used for path planning. When generating point-to-point trajectories and calculating flight time costs, it is crucial to take into account not only the potential risk of terrain collisions but also the need to avoid any threats posed by no-fly zones, thus ensuring the safety of the UAV.

### 3. Joint Planning Problem Formulation

#### 3.1. Safety Flight Topological Road Map

Before joint planning, the terrain data of the mission area are obtained through open sources. Based on the pre-acquired threat area ranges, data center coordinates, and pre-deployed reconnaissance node coordinates, an occupancy grid map is generated. The waypoints during the data collection process include the data center and the hovering collection positions of all reconnaissance nodes, denoted by  $\tilde{\mathcal{S}} = \mathcal{S} \cup s_{dc}$ . The flight trajectory between waypoints is represented by a series of discrete points, denoted by

$$W_{i,j}[r] = (x_{i,j}[r], y_{i,j}[r], h_{i,j}[r]), r = 1, 2, \dots, R_m \tag{13}$$

where  $W_{i,j}[1] = \omega_i, W_{i,j}[R_m] = \omega_j$ . The safety constraints include constraints on the mission area range, ground collision, maximum altitude, and no-fly zones.

The constraint on the mission area range represents the latitude and longitude constraints on the trajectory of the UAV, and it is expressed as

$$\begin{cases} 0 \leq x_{i,j}[r] \leq 1000 \\ 0 \leq y_{i,j}[r] \leq 1000 \end{cases} \tag{14}$$

The ground collision constraint and maximum altitude constraint primarily limit the altitude of the UAV during flight and are expressed as

$$h_t[r] \leq h_{i,j}[r] \leq h_t[r] + h_{\max} \tag{15}$$

where  $h_t[r]$  represents the altitude of the projected point of  $W_{i,j}[r]$  on the ground, and  $h_{\max}$  represents the maximum altitude of the UAV above ground level.

The flight safety constraint on the no-fly zone is denoted by

$$\|(x_{i,j}(r), y_{i,j}(r)) - (x_N, y_N)\| > r_N, \text{ if } h_{i,j}[r] \leq h_N \tag{16}$$

where the horizontal center coordinates are denoted by  $(x_N, y_N)$ , the radius is denoted by  $r_N$ , and the height is denoted by  $h_N$ .

On the basis of satisfying constraints (14)–(16), the path cluster represented by (13) is solved. This path cluster constitutes a topological road map for a safe UAV flight, which includes the optimal flight trajectories between every pair of nodes in  $\tilde{\mathcal{S}}$ .

#### 3.2. Joint Optimization of Reconnaissance Task Assignment and Node Access Sequence

First, we establish a graph model that represents the joint optimization problem, denoted by  $\mathcal{G} = (\tilde{\mathcal{S}}, \mathcal{E})$ . In this model, the set of waypoints for the reconnaissance UAV, denoted by  $\tilde{\mathcal{S}}$ , form the vertices of the graph.  $\mathcal{E}$  represents the edges of the graph, which are the set of safe flight trajectories between every pair of waypoints in the topological road map, denoted by  $\mathcal{E} = \{e_{i,j} | i, j \in 1, 2, \dots, N + 1\}$ . Therefore, the time cost of UAV flight on  $e_{i,j}$  can be represented as

$$c_{i,j} = \frac{1}{v_{avg}} \sum_{r=1}^{R_m-1} \|W_{i,j}[r+1] - W_{i,j}[r]\| \tag{17}$$

where  $v_{avg}$  represents the average flight speed of the UAV.

Due to the establishment of the topological road map, which provides the shortest flight paths between every pair of waypoints, repeated visits to the same node would increase the flight time. Therefore, the UAV departs from the data center and visits each reconnaissance node only once before returning to the data center. In a single-UAV reconnaissance scenario, the objective function is the average AoI of all reconnaissance node data. Based on (1)–(3), the following is obtained:

$$\begin{aligned}
 J_1 &= \frac{1}{N} \sum_{n=1}^N \Delta_{(n)}^* (T^{end}) \\
 &= \frac{1}{kN} \sum_{k=1}^5 \sum_{n \in \mathcal{S}_k} f_k \left( \sum_{i,i+1 \in \mathcal{S}_n \cup \mathcal{S}_0} (t_{i,i+1}^f + t_i^{dc}) \right)
 \end{aligned} \tag{18}$$

where  $\mathcal{S}_k$  represents the set of reconnaissance nodes with an information urgency of  $f_k$ , while  $\mathcal{S}_n$  represents the set of all nodes that come after node  $s_n$  in a certain sequence of reconnaissance node visits.

In a multi-UAV reconnaissance scenario, the objective function of this joint optimization problem is

$$\begin{aligned}
 J_2 &= \frac{1}{MN} \sum_{m=1}^M \sum_{n=1}^N \Delta_{(m,n)}^* (T_m^{end}) \\
 &= \frac{1}{M} \sum_{m=1}^M \frac{1}{kN} \sum_{k=1}^5 \sum_{n \in \mathcal{S}_{m,k}} f_k \left( \sum_{i,i+1 \in \mathcal{S}_{m,n} \cup \mathcal{S}_0} (t_{i,i+1}^f + t_i^{dc}) \right)
 \end{aligned} \tag{19}$$

The objective in (19) corresponds to using (18) to calculate the AAoI for each individual UAV and then obtaining the overall AAoI.

In addition, we also consider the heterogeneity of the collection terminals in the multi-UAV reconnaissance task allocation. We introduce the concept of “colors” from the colored traveling salesman problem (CTSP) to describe the correspondence between UAVs and heterogeneous reconnaissance nodes. Five different types of ground reconnaissance nodes are defined in Section 2.1, and among the multiple UAVs departing from the data center, some UAVs can only collect data from one type of node, while others can collect data from all types of nodes. This setting takes into account factors such as the models and the compatibility of data collection terminals in engineering practice, which may result in heterogeneity in the performance of UAVs in reconnaissance missions.

Let  $C = \{c_1, \dots, c_k, \dots, c_K\}$  represent the set of colors, where  $K$  is the number of different types of reconnaissance nodes with varying information urgency. The mapping between node types and colors is represented as follows:

$$c_k = f_C(n) \tag{20}$$

Therefore, the access constraints for heterogeneous UAVs can be represented as follows:

$$x_{i,j}^m = \begin{cases} 1, & f_C(j) \in C_m \\ 0, & \text{otherwise} \end{cases} \tag{21}$$

where  $x_{i,j}^m$  indicates that  $v_m$  immediately flies to the  $j$ -th node after completing data collection for the  $i$ -th reconnaissance node.  $C_m$  represents the color set assigned to  $v_m$ , satisfying  $C_m \in C$ , and in this paper, it is assumed to be a singleton set or the entire set.

### 3.3. Optimization Problem Formulation for Different Navigation Modes

In the VIO + GPS navigation mode, the autonomous UAV is able to obtain real-time and accurate self-positioning information. The GPS system can promptly correct the position

drift caused by accumulated VIO errors. In this mode, the optimization problem for the freshness of reconnaissance information for a single UAV can be formulated as follows:

$$(P1) \min_{W_{i,j}[r], x_{i,j}} J_1$$

$$s.t. \quad (8), (9), (14)–(16)$$

The optimization problem in multi-UAV scenarios incorporates the access constraints of heterogeneous data collection terminals. It can be formulated as

$$(P2) \min_{W_{i,j}[r], x_{i,j}^m} J_2$$

$$s.t. \quad (8), (9), (14)–(16), (21)$$

In the VIO + data collection and beacon-assisted positioning integration mode, the position drift of the UAV must be smaller than the maximum drift tolerance. According to [9], the magnitude of position drift is related to the flight distance between every two waypoints of the UAV. If the maximum drift amount  $\max(r_{c1}, r_{c2})$  corresponds to a maximum flight distance of  $c_{\max}$ , then in the modeling of the freshness optimization problem for single/multi-UAV reconnaissance information, waypoint selection constraints should also be included and denoted as

$$x_{i,j}^m = \begin{cases} 1, & c_{i,j} \leq c_{\max} \\ 0, & otherwise \end{cases} \quad (22)$$

In this case, the optimization problem for single/multi-UAV is, respectively, modeled as

$$(P3) \min_{W_{i,j}[r], x_{i,j}} J_1$$

$$s.t. \quad (8), (9), (14)–(16), (22)$$

$$(P4) \min_{W_{i,j}[r], x_{i,j}^m} J_2$$

$$s.t. \quad (8), (9), (14)–(16), (21), (22)$$

## 4. Algorithm Design

### 4.1. Calculation of Time Cost Matrix Based on A\* Algorithm

To address the mission and trajectory joint planning problem for single/multiple-UAV reconnaissance data collection in two different navigation modes, safe flight trajectories  $\{W_{i,j}[r]\}$  between waypoints are generated based on the A\* algorithm. A three-dimensional topological road map that satisfies safety constraints (14)–(16) is then constructed, and the flight time cost between waypoints is calculated using (17).

First, the three-dimensional space within the mission area is divided into uniformly continuous and non-overlapping grids, and the terrain and no-fly zone are annotated on the corresponding grids, forming the configuration space for the algorithm. Then, a heuristic search is conducted with the aim of minimizing the travel distance from the starting point of the current path segment until the destination grid is found. During the search process, the heuristic function of the current grid point is set as

$$g(r) = \lambda(r) + \theta(r) \quad (23)$$

where  $\lambda(r)$  represents the distance already traveled by the UAV from the starting point of the path segment to the current grid point, while  $\theta(r)$  represents the estimated travel distance from the current grid point to the end point of the path segment, which is set as the three-dimensional Euclidean distance. For the current grid point, the length of all

potential paths is greater than  $\theta(r)$ ; it can be concluded that this heuristic function exhibits consistency, and the flight trajectory generated is optimal in terms of the grid map. The overall process is illustrated in Algorithm 1. In the worst case, the complexity of the single A\* algorithm is  $\mathcal{O}(8^d)$ , where 8 is the number of child nodes during the node expansion, and  $d$  represents the number of steps in the shortest path from one waypoint to another. In practice, the A\* algorithm is often efficient because it effectively avoids evaluating unnecessary nodes.

---

**Algorithm 1:** Calculation of UAV safe flight trajectories and time cost matrix between waypoints based on A\* algorithm

---

- Input:** The digital elevation map within the mission area range, the set of reconnaissance nodes  $S$  and their coordinates  $\{\omega_n\}$ , the coordinates of the data center  $s_{dc}$ , the radius  $r_N$ , the height  $h_N$ , and the horizontal center coordinates  $(x_N, y_N)$  of the no-fly zone; set the maximum altitude above ground level  $h_{\max}$ .
- 3D Planning Space Configuration:** The grid-based obstacle representation with the reserved safety distance; set UAV motion degrees of freedom, including the horizontal longitude direction, horizontal latitude direction, vertical direction, and diagonal direction.
1. **Initialization:** Generate the vertex set  $\tilde{S}$ , define the time cost matrix  $\{c_{i,j}\}$ , define the open list  $OpenList$ , define the closed list  $CloseList$ , and define the candidate list  $CandiList$ .
  2. **Calculation process:**
  3. **for**  $i = 1$  to  $N + 1$  **do**
  4.   **for**  $j = 1$  to  $N + 1$  **do**
  5.     Set the starting point as  $\omega_i$ , set the ending point as  $\omega_j$ , set the visited list  $CloseList$  as empty, set the candidate list  $CandiList$  as empty, and reset the open list  $OpenList$ .
  6.     **while**  $OpenList \neq \emptyset$  **do**
  7.       **if**  $W_{i,j}[r] = \omega_j$  **then**
  8.         **break**
  9.       **end if**
  10.       Calculate the candidate path point list  $CandiList(t)$  based on the UAV motion degrees of freedom.
  11.       **for** all child nodes  $t$  **do**
  12.         **if**  $g(t + 1) = \inf$
  13.          $g(t + 1) = g(t) + \lambda(t, t + 1)$
  14.         Move  $CandiList(t + 1)$  from the open list to the visited list.
  15.         **elseif**  $g(t + 1) > g(t) + \lambda(t, t + 1)$
  16.          $g(t + 1) = g(t) + \lambda(t, t + 1)$
  17.         **endif**
  18.       **end for**
  19.     **end while**
  20.     Compute  $\{c_{i,j}\}$  based on (17).
  21. **end for**
  22. **end for**
- 

#### 4.2. Design of Heuristic Algorithm for Joint Optimization

Algorithm 1 constructs a safe flight topology roadmap to confine the UAV trajectory within safety constraints, thus simplifying the original optimization problem. In the VIO + GPS navigation mode, for the proposed single-UAV optimization problem, the hovering height is determined based on the communication distance constraint, and a modified intelligent optimization algorithm is used to solve the extended form of the classic single-agent TSP. This generates the visiting sequence for ground reconnaissance nodes, resulting in the final reconnaissance plan.

For the proposed multi-UAV optimization problem, the encoding stage of the intelligent optimization algorithm is designed in accordance with the heterogeneous UAV access constraints defined in (21). This establishes a joint solution space for reconnaissance mis-

sion assignment and visiting sequence optimization. The encoding scheme is illustrated in Algorithm 2. The simplified form of this algorithm is used to calculate the fitness function for the single-UAV optimization problem.

---

**Algorithm 2:** Encoding and fitness design for heuristic joint optimization algorithm

---

- Input:** The set of reconnaissance nodes  $\mathcal{S}$  and their coordinates  $\{\omega_n\}$ , the coordinates of the data center  $s_{dc}$ , urgency parameters  $\{\alpha_k\}$ , the time cost matrix  $\{c_{i,j}\}$ , and UAV identifiers  $\{v_m\}$ .
1. **Initialization:** Set the chromosome length to  $(N + M)$ , generate a random sequence  $route(N + M)$ , and create a temporary list  $TempList$ .
  2. Finding the index of the UAV's current location, denoted by  $index(m)$ .
  3. **Calculation process:**
  4. **for**  $m = 1$  to  $M$  **do**
  5.     **for**  $i = index(m)$  to  $index(m + 1)$  **do**
  6.         **if**  $f_C(i) \in C_m$
  7.             Adding  $route(i)$  to  $S_m$ .
  8.         **else**
  9.             Adding  $route(i)$  to  $TempList$ .
  10.         **end if**
  11.     **end for**
  12. **end for**
  13. Calculate the fitness of individuals using (19) based on the allocation results.
- 

In the VIO + data collection and beacon-assisted positioning integration mode, the waypoint selection constraint is derived from the maximum tolerance for position drift, as shown in (22). To enforce this constraint, a penalty function approach is adopted. In the fitness function of the intelligent optimization algorithm, which corresponds to the objectives in (18) and (19), a large penalty value is assigned to solutions that do not satisfy this constraint. This gradually eliminates infeasible solutions during the algorithm iteration. The complexity of intelligent optimization algorithms is mainly composed of fitness calculation, individual selection, and exploration strategy. Here,  $p$  represents the population size, and  $g$  represents the number of iterations. The computational complexity of the objective is  $\mathcal{O}(pN^2)$ , the computational complexity of individual selection is  $\mathcal{O}(p)$ , and during the exploration process, jump-point crossover, random mutation, and elite retention strategies are employed, with a computational complexity of  $\mathcal{O}(p)$ . Therefore, the complexity of the joint optimization is  $\mathcal{O}(gp * N^2)$ .

## 5. Numerical Results

In this section, we first implement the construction of a three-dimensional topological map for the UAV and estimate the flight time cost between waypoints. Then, based on this topological map, we address the joint planning problem for the autonomous navigation of single/multiple UAVs in different navigation modes. By comparing our proposed planning framework with the state of the art, we validate the rationality of our approach and the effectiveness of the corresponding algorithms. The simulation experiments were conducted using MATLAB R2021a.

### 5.1. Parameter Configuration and Generation of Safe Flight Topological Roadmap

Within a mission area of  $1000 \text{ m} \times 1000 \text{ m}$ , there is a heterogeneous set of nodes deployed for reconnaissance tasks. To simulate reconnaissance in mountainous environments that include peaks and valleys, where there may be risks of collision and electromagnetic interference, a portion of mountainous terrain was randomly extracted from ArcGIS 10.6 and preprocessed to generate the terrain described in this paper. No-fly zones are modeled as cylindrical regions, and entering these areas can result in exposure and potential hijacking, leading to mission failure.

In the simulation with randomly distributed nodes, we simulated scenarios with node quantities of 15, 30, and 45. In the scenario with regularly distributed nodes, there were 20 nodes. All nodes are classified into five different types, representing different types of reconnaissance data, which are depicted as diamond shapes of different colors in the figures. In order to ensure a realistic representation of the actual scenario, we take into account the spatial distribution of the nodes. Specifically, the coordinates of the nodes should exhibit randomness, but nodes of the same type should also exhibit a certain degree of spatial correlation.

The urgency parameter  $\alpha_k$  for these nodes is set according to Figure 1, ranging from urgent to less urgent. For nodes with an exponential, linear, and logarithmic growth of AoI, the amount of heterogeneous reconnaissance data collection is set to 1 Mbit, 2 Mbit, and 4 Mbit, respectively. Consequently, the corresponding hover collection times for these nodes are 1 s, 2 s, and 4 s. According to general logic, data with higher urgency typically have a smaller volume. For example, a 256-color RGB color image with a resolution of  $1280 \times 1024$  has a storage capacity close to 4 MB. This image may represent the parking situation in an outdoor parking lot from a fixed perspective, used to analyze the transport capacity, and the urgency of this information is relatively low. An electromagnetic spectrum sensor records signal strength data from different frequency bands, potentially generating a 2 MB dataset. These data can be used to analyze changes in enemy signal sources or interference, with moderate information urgency. A pressure sensor records traffic conditions on a specific road, potentially generating a 1 MB dataset. These data can be used to monitor enemy mobility status and detect potential invasion threats, with a higher level of information urgency.

The communication parameters in the simulations are set as follows. The data transmission bandwidth  $B$  for the low-power ground reconnaissance node is 1 MHz, and the transmission power  $p_t$  is 5 mW. The path loss exponent  $\alpha$  is 5, the noise power spectral density  $\sigma^2$  is  $-169$  dBm, the environmental parameter  $\mathcal{F}$  is 3, and the modulation and coding efficiency  $\Gamma$  is 1.5. Based on the UAV communication constraints (8)–(9), the maximum communication distance  $d_c$  is approximately 25 m. Considering flight safety, the UAV should stay away from unknown ground risks as much as possible. Therefore, the hover collection altitude  $h_{dc}$  for the UAV is set to 20 m.

The field-of-view angle  $2\eta$  of the camera below the UAV is set to  $80^\circ$ , and based on (10),  $r_{c1}$  is approximately 16.78 m. Based on (12),  $r_{c2}$  is approximately 15 m. Referring to [12], a VIO autonomous navigation UAV will have a position drift of 1 m after flying for around 37 m. Therefore, to ensure that the position drift is smaller than the error tolerance radius  $\max(r_{c1}, r_{c2})$  after a certain flying time, the maximum flight distance  $c_{\max}$  satisfying the waypoint selection constraint (22) is approximately 600 m. In other words, the maximum flight time cost for satisfying the waypoint selection constraint is  $c_{i,j} \leq 600$  m.

Figure 4 illustrates the distribution of these heterogeneous nodes in the mission area and the UAV safe flight topological roadmap constructed using Algorithm 1. Among them, the deep-red nodes represent the hovering collection positions corresponding to nodes with an urgency parameter of  $\alpha = 0.005$ ; the light-red nodes correspond to  $\alpha = 0.025$ ; the green nodes correspond to  $\alpha \rightarrow 0$ ; the blue nodes correspond to  $\alpha = -0.025$ ; and the white nodes correspond to  $\alpha = -0.005$ . In addition, the black pentagon represents the data center, and the dark lines represent the safe flight topological roadmap formed by the optimal paths between each two waypoints. Based on this, the joint planning of missions and paths for autonomous navigation UAVs in different navigation modes is further implemented using Algorithm 2.

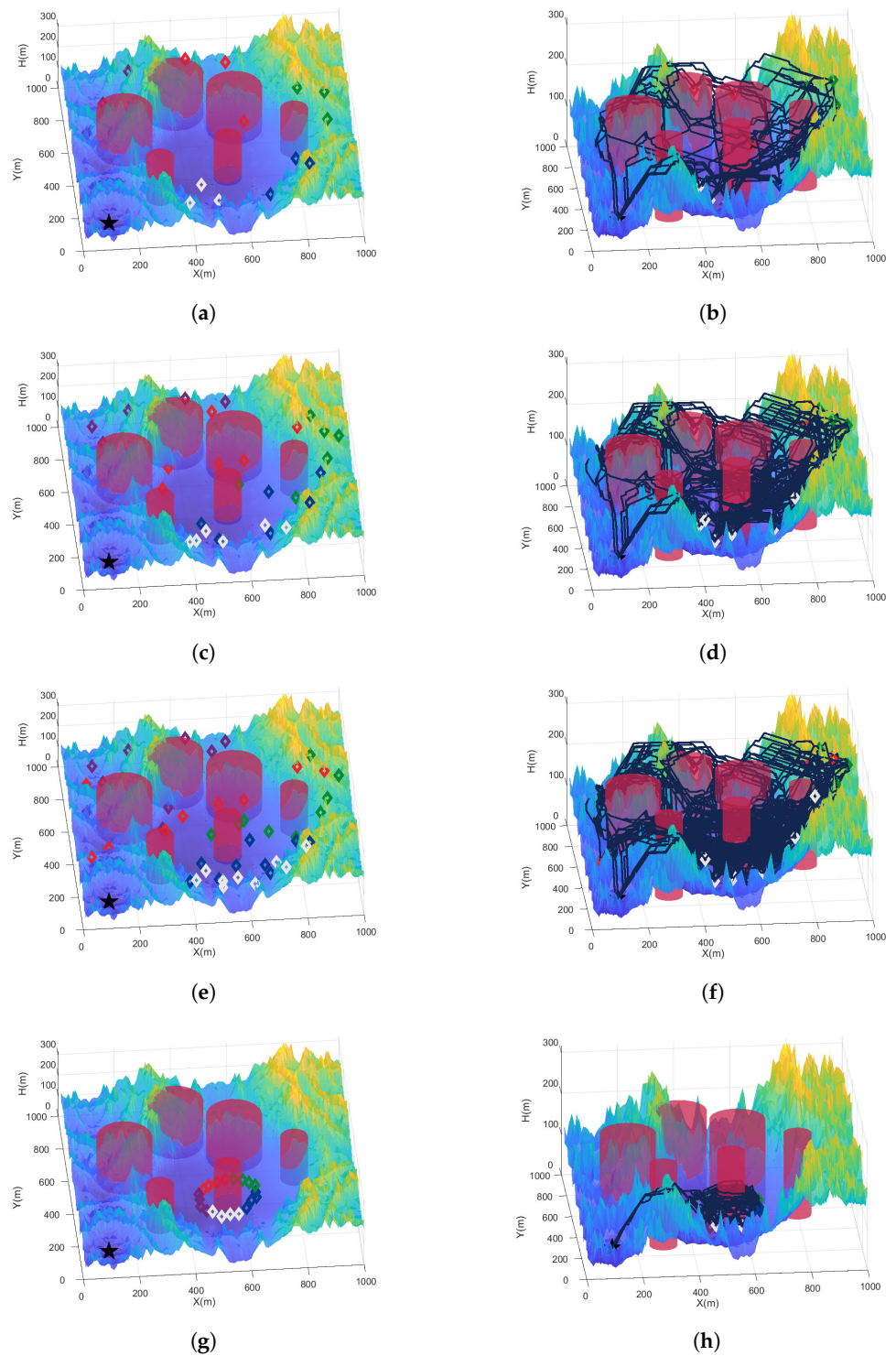


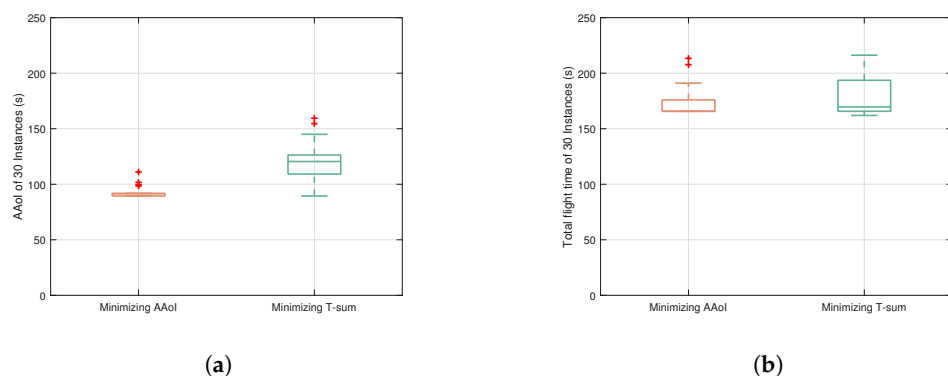
**Figure 4.** Nodes and mission environment schematic diagram, along with corresponding three-dimensional topological roadmap. (a) Random distribution of 15 nodes. (b) Topological roadmap of 15 nodes. (c) Random distribution of 30 nodes. (d) Topological roadmap of 30 nodes. (e) Random distribution of 45 nodes. (f) Topological roadmap of 45 nodes. (g) Circular distribution of 20 nodes. (h) Topological roadmap of 20 nodes.

### 5.2. Simulations of VIO + GPS Navigation Mode

The main objective of the heuristic optimization algorithm designed in this paper is to effectively improve the timeliness of reconnaissance information, which is characterized by the information freshness with heterogeneous urgency, as proposed in (3). In order

to achieve this under complex constraints, direct optimization schemes, as well as the minimizing total flight time scheme and minimizing mission duration scheme proposed in [16], are adopted and extensively compared and analyzed. In the following simulations, two navigation modes are applied in different conditions. The first is the VIO + GPS mode, corresponding to (P1) and (P2) when GPS is available; the second is the VIO + data collection and beacon-assisted positioning integration mode, corresponding to (P3) and (P4) when GPS is unavailable due to the existence of interference or hijacking.

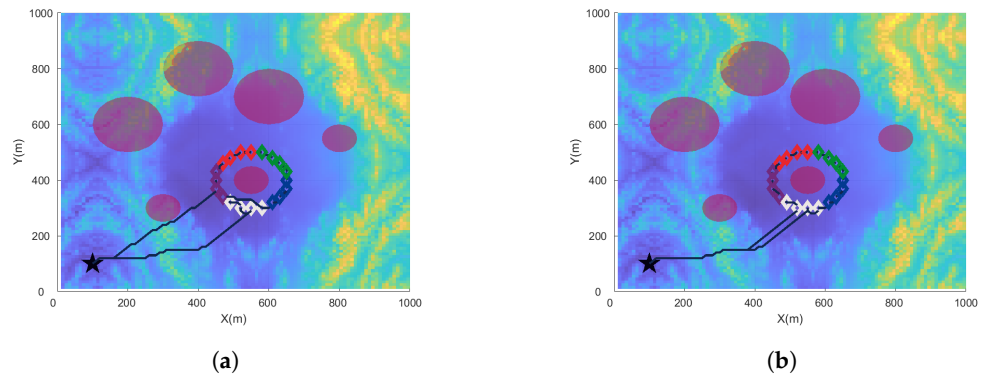
Figure 5 presents the results of 30 Monte Carlo simulations showcasing the optimization of information freshness for a single UAV in VIO + GPS navigation mode using box plots. In this simulation, the direct optimization scheme aims to minimize the AAoI of reconnaissance nodes and is denoted as “Minimizing AAoI”, while the minimizing total flight time scheme aims to minimize the overall UAV flight time and is denoted as “Minimizing T-sum”. The simulation scenario involves 20 nodes distributed in a nearly circular pattern from the top view. It can be observed that in scenarios with a regular distribution of reconnaissance nodes, both the direct optimization scheme and the minimizing total flight time scheme yield stable results. The direct optimization scheme shows slightly improved and more stable performance in terms of the AAoI and total flight time metrics. This can be attributed to the better guidance provided by the heterogeneous information urgency in scenarios with regularly distributed nodes.



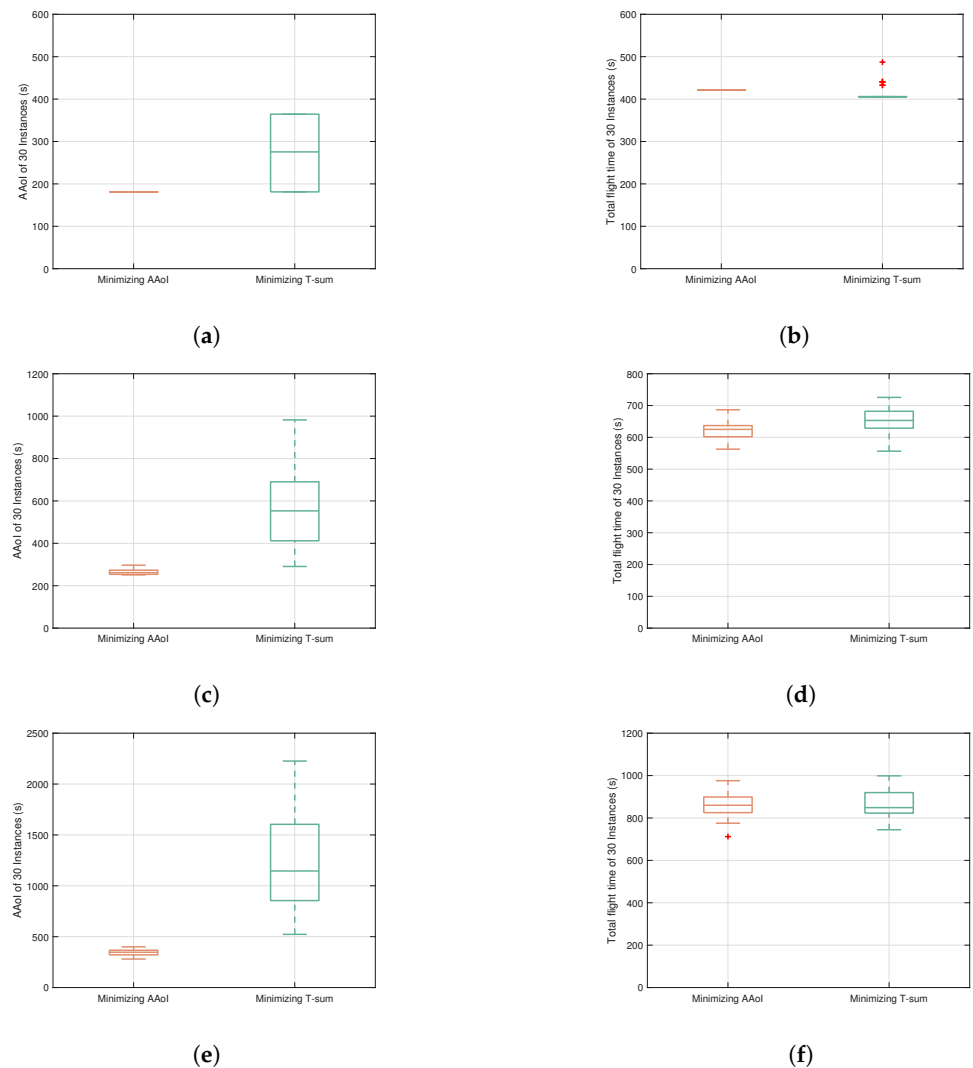
**Figure 5.** The comparative results of 30 Monte Carlo simulations between the direct optimization scheme and the minimum total flight time scheme in the scenario of ground reconnaissance nodes with a regular distribution, where the red crosses represent outliers caused by the optimization algorithm getting trapped in local optima. (a) A box plot comparing the AAoI metric. (b) A box plot comparing the total flight time metric.

Figure 6 displays the planning results near the median values in the box plots. From the calculated paths, it is evident that the direct optimization scheme considers both terrain and no-fly zones, as well as the heterogeneous urgency of nodes, making it a preferable choice in similar scenarios with a regular distribution of reconnaissance nodes.

Figure 7 presents the simulation results using box plots for scenarios with random distributions of 15, 30, and 45 nodes. It can be observed that when the distribution of reconnaissance nodes lacks geometric regularity, the direct optimization scheme achieves superior and more stable performance. Both the proposed AAoI metric with heterogeneous information urgency and the traditional total flight time metric demonstrate improved performance with the direct optimization approach. This is attributed to the non-linear growth rate of AoI proposed in this paper, which guides the optimization direction during the iterative process of the intelligent optimization algorithm.



**Figure 6.** A comparison of results with target values near the median. (a) The path planned for the direct optimization scheme. (b) The path planned for the total flight time minimization scheme.



**Figure 7.** Comparing the results of 30 Monte Carlo simulations between the direct optimization scheme and the total flight time minimization scheme in a scenario where ground reconnaissance nodes are randomly distributed. (a) A box plot comparing the AAoI metric in a scenario with 15 nodes. (b) A box plot comparing the total flight time metric in a scenario with 15 nodes. (c) A box plot comparing the AAoI metric in a scenario with 30 nodes. (d) A box plot comparing the total flight time metric in a scenario with 30 nodes. (e) A box plot comparing the AAoI metric in a scenario with 45 nodes. (f) A box plot comparing the total flight time metric in a scenario with 45 nodes.

Comparing the results in Figure 8, where the target values are close to the median, it is evident that as the number of nodes increases, the non-linear growth rate provides more distinct guidance for the optimization direction, resulting in more reasonable computational results. Therefore, in this scenario, utilizing the intelligent optimization algorithm and the direct optimization approach proposed in this study can lead to fresher reconnaissance information.

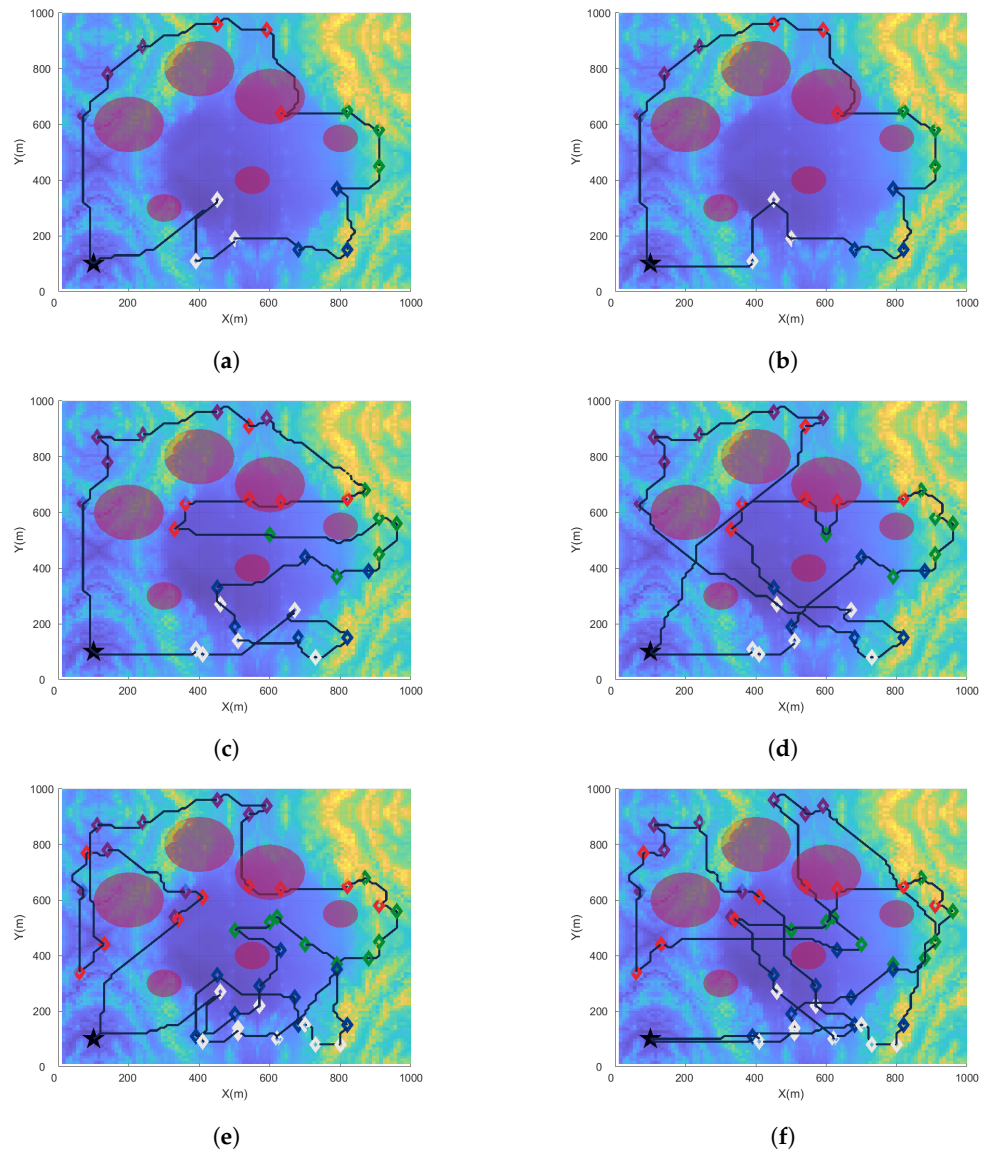


**Figure 8.** A comparison of results with target values near the median. (a) The planned path of the direct optimization scheme in the scenario with 15 nodes. (b) The planned path of the total flight time minimization scheme in the scenario with 15 nodes. (c) The planned path of the direct optimization scheme in the scenario with 30 nodes. (d) The planned path of the total flight time minimization scheme in the scenario with 30 nodes. (e) The planned path of the direct optimization scheme in the scenario with 45 nodes. (f) The planned path of the total flight time minimization scheme in the scenario with 45 nodes.

5.3. Simulations of VIO + Data Collection and Beacon-Assisted Positioning Integration Mode

For the VIO + data collection and beacon-assisted positioning integration mode, (P3) has a penalty term added to the fitness in order to enforce waypoint selection constraints that satisfy the maximum allowable position drift in a soft constraint manner. However, utilizing the direct optimization scheme and the minimizing total flight time scheme may

not always successfully plan a safe path that meets the maximum allowable position drift constraint, as intelligent optimization algorithms themselves are prone to getting trapped in local optima. Hence, a combined scheme was adopted in simulations, where the fitness function combined the reconnaissance node AAOI and total flight time information to achieve a better optimization of reconnaissance information freshness.

Table 1 presents the success rates of intelligent optimization algorithms when employing three different schemes for (P3). In a scenario with 15 randomly distributed nodes, the sparse distribution of nodes makes it challenging to meet the maximum allowable position drift constraint, resulting in instances where all three schemes fail to successfully plan a path, indicating the possibility of the UAV getting lost due to position drift. Among the schemes, the direct optimization scheme has the highest failure rate, attributed to the non-linear urgency of information proposed in this study causing drastic changes in AoI growth rates, leading to the penalty value of the fitness function becoming ineffective during the iteration process of the intelligent optimization algorithms.

**Table 1.** The success rate of the intelligent optimization scheme for a single UAV in the navigation mode of VIO + data collection and beacon-assisted positioning integration.

Number of Nodes	Optimization Scheme	Planning Success Rate
15	Minimizing AAOI	20%
	Minimizing T-sum	73%
	Combined Scheme	67%
30	Minimizing AAOI	53%
	Minimizing T-sum	100%
	Combined Scheme	100%
45	Minimizing AAOI	27%
	Minimizing T-sum	100%
	Combined Scheme	100%

The success rate of the minimizing total flight time scheme and the proposed combined scheme has shown significant improvement compared to the direct optimization scheme. In 30- and 45-node scenarios, all 30 Monte Carlo simulations resulted in a 100% success rate. In contrast, the direct optimization scheme still experienced numerous planning failures in these scenarios.

A further comparison of the numerical results for the combined scheme and the minimizing total flight time scheme in this scenario, as shown in Figure 9, demonstrates that the combined scheme exhibits a significant advantage in both the AAOI and total flight time metrics. This is considered the optimal solution for this scenario.

In the scenario (P2) representing multi-UAV reconnaissance, we conducted numerical simulations on the randomly distributed scenario with 45 nodes. It is assumed that a total of seven UAVs are dispatched to collect reconnaissance data from the nodes. Among them, five UAVs correspond to five different types of ground nodes, denoted by the color sets  $\{c_1\}$ ,  $\{c_2\}$ ,  $\{c_3\}$ ,  $\{c_4\}$ , and  $\{c_5\}$  in constraint (21), while the other two UAVs correspond to all types of ground nodes, represented by the color set  $\{c_1, c_2, c_3, c_4, c_5\}$ . In the multi-UAV reconnaissance scenario, in addition to the previously mentioned direct optimization scheme (Minimizing AAOI) and minimizing total flight time scheme (Minimizing T-sum), we also employed the minimizing maximum flight time scheme, also known as the minimizing total mission duration scheme, denoted as Minimizing T-max.

Figure 10 presents the timeliness performance of these three schemes for reconnaissance information, as shown by the box plots. Although there are certain differences in performance and stability between the direct optimization scheme and the minimizing maximum flight time scheme, both schemes achieve acceptable results in terms of information timeliness and total mission duration compared to the minimizing total flight time scheme.

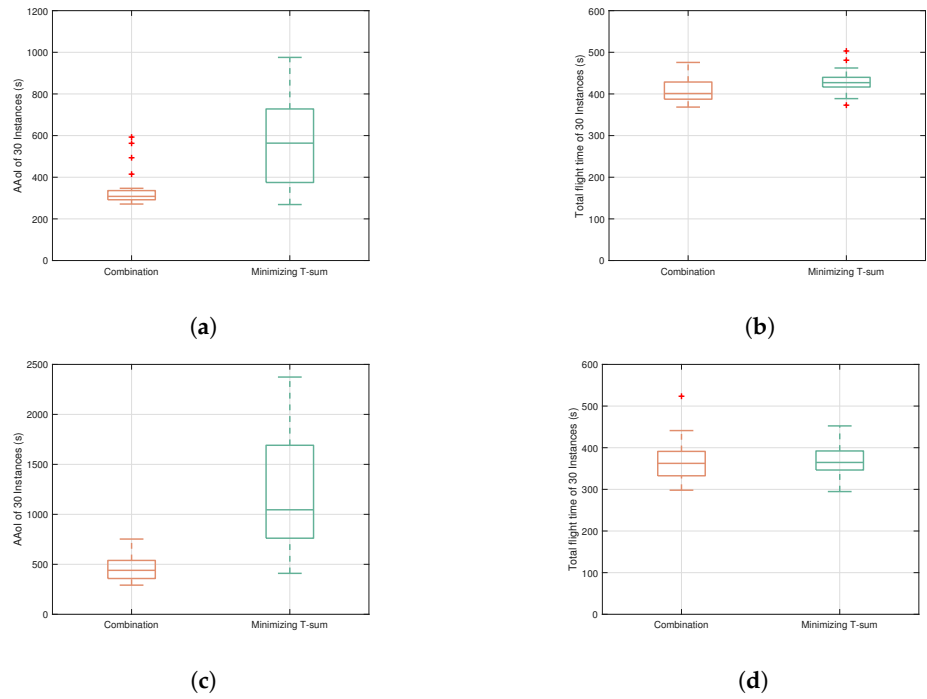


**Figure 9.** Comparing the results of 30 Monte Carlo simulations between the combined scheme and the total flight time minimization scheme in the VIO + data collection and beacon-assisted integrated navigation mode. (a) A box plot comparing the AAoI metric in a scenario with 30 nodes. (b) A box plot comparing the total flight time metric in a scenario with 30 nodes. (c) A box plot comparing the AAoI metric in a scenario with 45 nodes. (d) A box plot comparing the total flight time metric in a scenario with 45 nodes.

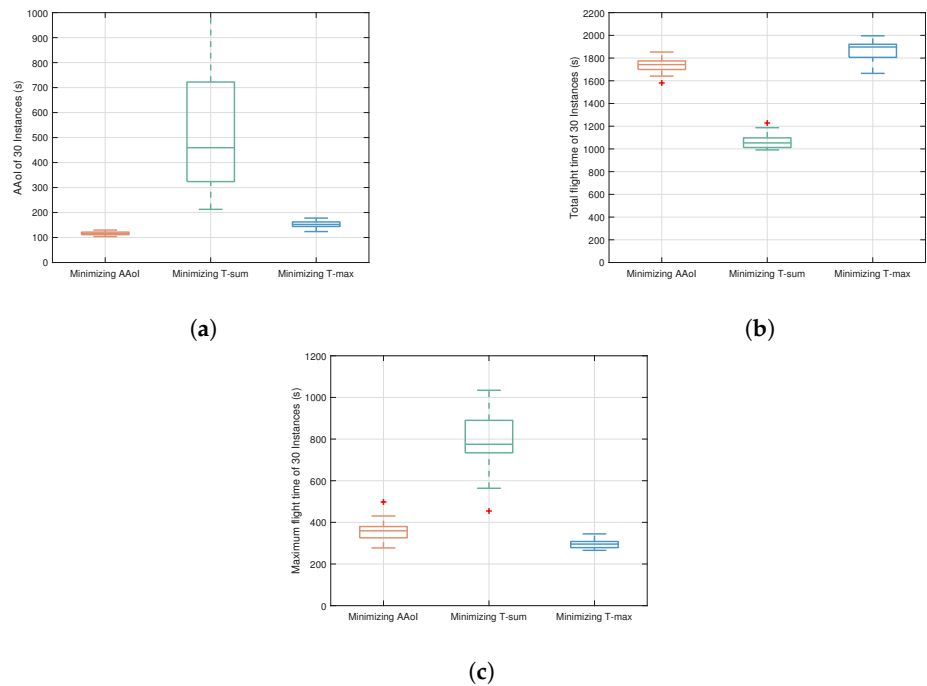


**Figure 10.** Comparing the results of 30 Monte Carlo simulations for the direct optimization scheme, minimizing total flight time scheme, and minimizing total mission duration scheme in the VIO + GPS navigation mode. (a) A box plot comparing the AAoI metric in multi-UAV reconnaissance. (b) A box plot comparing the total flight time metric in multi-UAV reconnaissance. (c) A box plot comparing the maximum flight time metric in multi-UAV reconnaissance.

From the planning results in Figure 11, where the objective values are near the median, it can be observed that the direct optimization scheme and the minimizing maximum flight time scheme yield more similar planning outcomes. However, the minimizing total flight time scheme unevenly distributes the tasks to a small number of UAVs, compromising the timeliness of the reconnaissance information. Therefore, it is not suitable for this scenario.

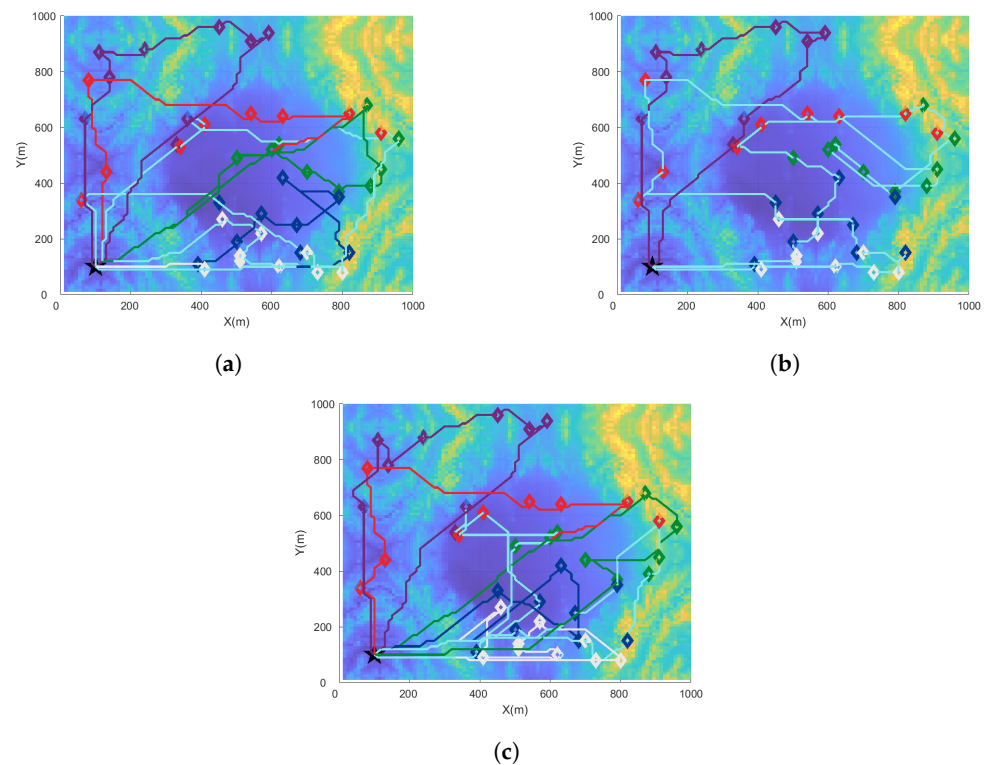


**Figure 11.** A comparison of results with target values near the median. The paths of UAVs corresponding to five different types of ground nodes are represented by lines of respective colors. Meanwhile, the paths of UAVs corresponding to all types of ground nodes are represented by light blue lines. (a) The planned path of the direct optimization scheme. (b) The planned path of the minimizing total flight time scheme. (c) The planned path of the minimizing maximum flight time scheme.

Furthermore, comparing the results in Figure 10 with those in Figure 7, it can be concluded that the use of multiple UAVs effectively reduces the AAoI of the reconnaissance nodes, thus improving its information freshness. This finding aligns with the expected conclusion. In this scenario, the direct optimization scheme shows a slight advantage over the total flight time minimization scheme.

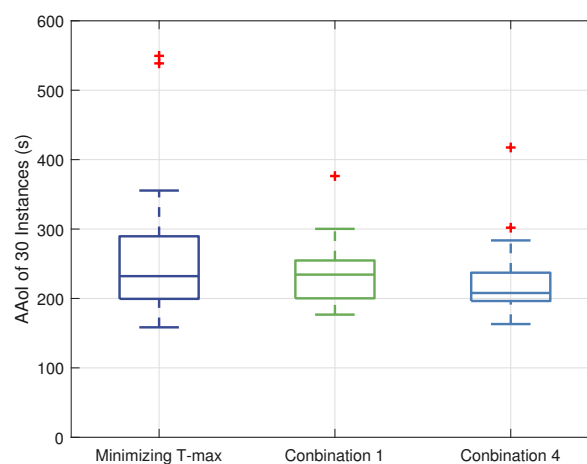
For the integrated VIO + data collection and beacon-assisted localization navigation mode, the penalty function method is also adopted in (P4) to enforce the constraint on the maximum drift tolerance in positioning. In Table 2, it can be observed that the direct optimization scheme struggles to achieve effective planning results for this problem. Therefore, in addition to the three aforementioned schemes, different joint planning schemes are also compared. Joint scheme 1 involves designing optimization objectives that simultaneously consider the AAoI and total flight time indicators, joint scheme 2 considers the AAoI and total mission duration, joint scheme 3 considers the total flight time and total mission duration, and joint scheme 4 simultaneously considers all three factors. Table 2 displays the success rates of all planning schemes in this scenario, with the minimizing maximum flight time scheme, joint scheme 1, and joint scheme 4 showing relatively acceptable success rates. Through the analysis of (P2), it is evident that the performance of the AAoI for the minimizing total flight time scheme and joint scheme 3 is unacceptable, and therefore, they are no longer considered.

**Table 2.** The success rate of the intelligent optimization scheme for multiple UAVs in the navigation mode of VIO + data collection and beacon-assisted positioning integration.

Number of Nodes	Optimization Scheme	Planning Success Rate
45	Minimizing AAOI	0%
	Minimizing T-sum	90%
	Minimizing T-max	100%
	Joint scheme 1	83%
	Joint scheme 2	37%
	Joint scheme 3	73%
	Joint scheme 4	77%

In this scenario, joint schemes 1 and 4 improve the AAOI indicator to a certain extent but also carry a certain risk of position drift, which may cause the partial loss of UAVs and the incomplete execution of reconnaissance missions. The performance of joint scheme 4 is slightly better than that of joint scheme 1, but the risk is also slightly higher.

Comparing Figures 9 and 12, it can be concluded that assigning multiple UAVs also improves the overall freshness of reconnaissance information in the integrated VIO + data collection and beacon-assisted localization navigation mode. However, there is a tradeoff between risk and performance when selecting a scheme, and a compromise should be made based on the specific reconnaissance mission.

**Figure 12.** The Monte Carlo simulation results for the integrated VIO + data collection and beacon-assisted localization navigation mode, comparing the minimizing maximum flight time scheme, joint scheme 1, and joint scheme 4.

## 6. Conclusions

This study focuses on the characteristics of autonomous UAVs in different navigation modes and investigates the autonomous mission and joint path planning problems for single/multiple UAVs. Through the designed optimization scheme, the freshness of reconnaissance information is effectively enhanced. Extensive numerical simulations were conducted in MATLAB to evaluate the success rate and effectiveness of the planning schemes in each scenario, highlighting the selection of the optimal solution and the trade-off between the success rate and timeliness. In future work, the framework of intelligent optimization algorithms will be improved, and the algorithmic exploration process will be further explored to achieve performance improvements. Additionally, the authors will strive to port the proposed planner from MATLAB to the ROS system and conduct real-world validation experiments in the future.

**Author Contributions:** Conceptualization, C.X.; Methodology, C.X., B.W. and D.G.; Software, C.X. and B.W.; Validation, C.X., B.W. and D.G.; Formal Analysis, C.X. and X.C.; Investigation, D.G. and X.C.; Resources, B.W. and D.G.; Data Curation, C.X., B.W. and D.G.; Writing—Original Draft, C.X.; Writing—Review and Editing, B.W., D.G. and X.C.; Visualization, B.W.; Supervision, B.W., D.G. and X.C.; Project Administration, D.G. and X.C.; Funding Acquisition, D.G. and X.C. All authors have read and agreed to the published version of the manuscript.

**Funding:** This research was supported in part by the National Natural Science Foundation of China (NSFC) (No. 62101273).

**Data Availability Statement:** The data presented in this study are available on request from the corresponding author.

**Conflicts of Interest:** The authors declare no conflicts of interest.

## Abbreviations

The following abbreviations are used in this manuscript:

UAV	Unmanned aerial vehicle
IMU	Inertial measurement unit
SLMM	Simultaneous localization and mapping
UWB	Ultra-wideband
VIO	Visual-inertial odometry
ECTSP	Extended colored traveling salesman problem
AoI	Age of information
AAoI	Average age of information
LoS	Line-of-sight
NLoS	Non-line-of-sight
DEM	Digital elevation model
CTSP	Colored traveling salesman problem

## References

- Jiang, H.; Zhang, Z.; Dang, J.; Wu, L. Analysis of geometric multibounced virtual scattering channel model for dense urban street environments. *IEEE Trans. Veh. Technol.* **2017**, *66*, 1903–1912. [[CrossRef](#)]
- Jiang, H.; Zhang, Z.; Wu, L.; Dang, J. Novel 3-D irregular-shaped geometry-based channel modeling for semi-ellipsoid vehicle-to-vehicle scattering environments. *IEEE Wireless Commun. Lett.* **2018**, *7*, 836–839. [[CrossRef](#)]
- Lin, P.; Ning, Z.; Zhang, Z.; Liu, Y.; Yu, F.R.; Leung, V.C. Joint optimization of preference-aware caching and content migration in cost-efficient mobile edge networks. *IEEE Trans. Wireless Commun.* **2023**. [[CrossRef](#)]
- Jiang, H.; Xiong, B.; Zhang, H.; Basar, E. Physics-based 3D end-to-end modeling for double-RIS assisted non-stationary UAV-to-ground communication channels. *IEEE Trans. Commun.* **2023**, *71*, 4247–4261. [[CrossRef](#)]
- Xiong, B.; Zhang, Z.; Jiang, H. Reconfigurable intelligent surface for mmwave mobile communications: What if LoS path exists? *IEEE Wireless Commun. Lett.* **2023**, *12*, 247–251. [[CrossRef](#)]
- Ruan, C.; Zhang, Z.; Jiang, H.; Dang, J.; Wu, L.; Zhang, H. Approximate message passing for channel estimation in reconfigurable intelligent surface aided MIMO multiuser systems. *IEEE Trans. Commun.* **2022**, *70*, 5469–5481. [[CrossRef](#)]
- Wu, B.; Guo, D.; Zhang, B.; Zhang, X.; Wang, H.; Wang, H.; Jiang, H. Completion time minimization for UAV enabled data collection with communication link constrained. *IET Commun.* **2022**, *16*, 1025–1040. [[CrossRef](#)]
- Wu, B.; Zhang, B.; Guo, D.; Wang, H.; Jiang, H. Anti-jamming trajectory design for UAV-enabled wireless sensor networks using communication flight corridor. *China Commun.* **2022**, *19*, 37–52. [[CrossRef](#)]
- Zhou, X.; Wen, X.; Wang, Z.; Gao, Y.; Li, H.; Wang, Q.; Yang, T.; Lu, H.; Cao, Y.; Xu, C.; et al. Swarm of micro flying robots in the wild. *Sci. Robot.* **2022**, *7*, eabm5954. [[CrossRef](#)] [[PubMed](#)]
- Wu, B.; Zhang, B.; Ma, W.; Xie, C.; Guo, D.; Jiang, H. Motion planning in UAV-aided data collection with dynamic jamming. *Electronics* **2023**, *12*, 1841. [[CrossRef](#)]
- Zhou, B.; Pan, J.; Gao, F.; Shen, S. RAPTOR: Robust and perception-aware trajectory replanning for quadrotor fast flight. *IEEE Trans. Robot.* **2021**, *37*, 1992–2009. [[CrossRef](#)]
- Xu, H.; Zhang, Y.; Zhou, B.; Wang, L.; Yao, X.; Meng, G.; Shen, S. Omni-swarm: A decentralized omnidirectional visual-inertial-UWB state estimation system for aerial swarms. *IEEE Trans. Robot.* **2022**, *38*, 3374–3394. [[CrossRef](#)]
- Jiang, H.; Zhang, Z.; Wu, L.; Dang, J.; Gui, G. A 3-D non-stationary wideband geometry-based channel model for MIMO vehicle-to-vehicle communications in tunnel environments. *IEEE Trans. Veh. Technol.* **2019**, *68*, 6257–6271. [[CrossRef](#)]
- Jiang, H.; Zhang, Z.; Dang, J.; Wu, L. A novel 3-D massive MIMO channel model for vehicle-to-vehicle communication environments. *IEEE Trans. Commun.* **2018**, *66*, 79–90. [[CrossRef](#)]

15. Zeng, L.; Liao, X.; Ma, Z.; Xiong, B.; Jiang, H.; Chen, Z. Three-dimensional UAV-to-UAV channels: Modeling, simulation, and capacity analysis. *IEEE Internet Things J.* **2023**, *11*, 10054–10068. [[CrossRef](#)]
16. Miloradović, B.; Çürüklü, B.; Ekström, M.; Papadopoulos, A.V. GMP: A genetic mission planner for heterogeneous multirobot system applications. *IEEE Trans. Cybern.* **2022**, *52*, 10627–10638. [[CrossRef](#)] [[PubMed](#)]
17. Hu, H.; Xiong, K.; Qu, G.; Ni, Q.; Fan, P.; Letaief, K.B. AoI-minimal trajectory planning and data collection in UAV-assisted wireless powered IoT networks. *IEEE Internet Things J.* **2021**, *8*, 1211–1223. [[CrossRef](#)]
18. Xiong, B.; Zhang, Z.; Jiang, H.; Zhang, J.; Wu, L.; Dang, J. A 3D non-stationary MIMO channel model for reconfigurable intelligent surface auxiliary UAV-to-ground mmwave communications. *IEEE Trans. Wireless Commun.* **2022**, *21*, 5658–5672. [[CrossRef](#)]
19. Fu, J.; Sun, G.; Liu, J.; Yao, W.; Wu, L. On hierarchical multi-UAV dubins traveling salesman problem paths in a complex obstacle environment. *IEEE Trans. Cybern.* **2023**, *54*, 123–135. [[CrossRef](#)] [[PubMed](#)]
20. Miridakis, N.I.; Tsiftsis, T.A.; Yang, G. Non-linear age of information: An energy efficient receiver-centric approach. *IEEE Wireless Commun. Lett.* **2022**, *11*, 655–659. [[CrossRef](#)]
21. Jiang, H.; Zhang, Z.; Wu, L.; Dang, J. Three-dimensional geometry-based UAV-MIMO channel modeling for A2G communication environments. *IEEE Commun. Lett.* **2018**, *22*, 1438–1441. [[CrossRef](#)]
22. Xiong, B.; Zhang, Z.; Ge, Y.; Wang, H.; Jiang, H.; Wu, L.; Zhang, Z. Channel modeling for heterogeneous vehicular ISAC system with shared clusters. In Proceedings of the IEEE 98th Vehicular Technology Conference (VTC2023-Fall), Hong Kong, 10–13 October 2023; pp. 1–6. [[CrossRef](#)]
23. Liu, T.; Jiang, H.; Chen, Z.; Zhang, H.; Yang, X.; Shu, F. Nonlinear channel estimation and signal detection for quantized OFDM system. *IEEE Commun. Lett.* **2023**, *27*, 2772–2776. [[CrossRef](#)]
24. Jiang, H.; Zhang, Z.; Wang, C.X.; Zhang, J.; Dang, J.; Wu, L.; Zhang, H. A novel 3D UAV channel model for A2G communication environments using AoD and AoA estimation algorithms. *IEEE Trans. Commun.* **2020**, *68*, 7232–7246. [[CrossRef](#)]
25. Gong, Z.; Wu, L.; Zhang, Z.; Dang, J.; Zhu, B.; Jiang, H.; Li, G.Y. Joint TOA and DOA estimation with CFO compensation using large-scale array. *IEEE Trans. Signal Process.* **2021**, *69*, 4204–4218. [[CrossRef](#)]

**Disclaimer/Publisher’s Note:** The statements, opinions and data contained in all publications are solely those of the individual author(s) and contributor(s) and not of MDPI and/or the editor(s). MDPI and/or the editor(s) disclaim responsibility for any injury to people or property resulting from any ideas, methods, instructions or products referred to in the content.